



# Seismic attenuation near the East Pacific Rise and the origin of the low-velocity zone

Yingjie Yang<sup>a,\*</sup>, Donald W. Forsyth<sup>a</sup>, Dayanthie S. Weeraratne<sup>b</sup>

<sup>a</sup> Department of Geological Sciences, Brown University, Providence, Rhode Island 02912, United States

<sup>b</sup> Department of Terrestrial Magnetism, Carnegie Institution of Washington, Washington, DC 20015-1305, United States

Received 22 August 2006; received in revised form 22 March 2007; accepted 22 March 2007

Editor: R.D. van der Hilst

## Abstract

Low shear wave velocities beneath mid-ocean ridges and in the low-velocity zone beneath oceanic plates commonly have been attributed to the presence of melt or dissolved water, but several recent studies have challenged that interpretation. The alternative is that the anelastic effects of increasing temperature may cause the observed drop in velocity along with a predicted increase in attenuation. We report the first measurements of surface wave attenuation within regional arrays of seismometers on the seafloor. Near the East Pacific Rise, there is much less attenuation than is predicted by models in which the velocity is controlled solely by the direct elastic and anelastic effects of changing temperature, suggesting that melt and water concentration do play an important role. There also is somewhat less attenuation than is found in global studies; we speculate that scattering from unresolved velocity heterogeneities contribute to the apparent attenuation in global studies.

© 2007 Elsevier B.V. All rights reserved.

**Keywords:** East Pacific Rise; asthenosphere; low-velocity zone; surface waves; attenuation

## 1. Introduction

One of the crucial questions in plate tectonics is the origin of the low-velocity zone (LVZ) in the upper mantle. The LVZ is also a layer of high attenuation of seismic waves, low viscosity and high electrical conductivity [1] and is thus commonly associated with the asthenosphere. The low viscosity asthenosphere can lubricate the motion of the cold, highly viscous or elastic overlying plates and thus may be the key factor that leads to convection in the earth taking the form of plate tectonics [2]. Because the factors controlling velocity

and attenuation of seismic waves probably also control the rheology of the mantle materials, a better understanding of origin of the LVZ can help us to understand the interaction between the lithosphere and sub-lithosphere upper mantle.

Early studies attributed the pronounced oceanic low-velocity zone to the presence of partial melt in the upper mantle [3]. Karato and Jung [4] argued that higher water content in the asthenosphere significantly reduces the seismic wave velocities through anelastic relaxation. More recently, however, several studies have suggested that the increase in temperature with depth is sufficient to explain the origin of the LVZ if anelastic effects are taken into account [5–7] and neither water nor melt is required. In addition, the very

\* Corresponding author.

E-mail address: [yingjie.yang@colorado.edu](mailto:yingjie.yang@colorado.edu) (Y. Yang).

low shear velocities beneath spreading, mid-ocean ridges were also attributed primarily [6] or entirely [7] to high temperatures in the upwelling mantle. Although there must be some melt present in the mantle beneath mid-ocean ridges to supply the magma that forms new oceanic crust at spreading centers, it may be efficiently extracted, leaving too small a melt fraction to have significant effect on the seismic velocities [7]. Because the anelasticity thought to be responsible for reducing the velocity also causes attenuation of seismic waves, measurements of the decay of the amplitude of seismic surface waves sensitive to lithospheric and asthenospheric structure provide a means of testing these models for the origin of the low-velocity zone.

It is, however, difficult to measure the attenuation of seismic waves reliably due to the problem of separating intrinsic attenuation effects on amplitude from other effects such as scattering or focusing/defocusing caused by elastic heterogeneities. Inverting for attenuation without considering focusing can introduce systematic bias, sometime even resulting in negative apparent attenuation. Recently, with the development of finite-frequency scattering theory for surface waves [8], Yang and Forsyth [9] developed a regional-scale surface wave tomography method that accounts for scattering or focusing by velocity heterogeneities within the study area using the Born approximation and represents the first-order effects of scattering between the source and the study area as the interference between two plane waves. In addition, terms are included that correct for the amplitude response or site response at each station. By using many stations and sources at a variety of azimuths, we can detect the velocity heterogeneities that cause focusing and so we can separate the scattering and focusing/defocusing effects on amplitude from attenuation.

In this study, we simultaneously invert for lateral variations in phase velocities and attenuation coefficients in very young seafloor (less than 10 Ma) using phase and amplitude data of fundamental mode Rayleigh waves. The attenuation coefficients are used to invert for  $Q_\mu$  in the upper mantle. Shear wave  $Q_\mu$  and velocities are used together to constrain the formation of the oceanic plate and the origin of the low-velocity zone (LVZ) in the oceanic mantle.

## 2. Methodology and data processing

In our inversion, we solve for lateral changes in phase velocity simultaneously with attenuation in order to account for focusing effects. Attenuation is assumed to be a function only of distance of propagation  $x$  in the form  $e^{-\gamma x}$ , while we use the full 2-D, finite frequency

response kernels for phase velocity and focusing. Another factor affecting amplitude is station site response owing to the difference in structure beneath each station or slight differences in seismometer response. We include an additional amplitude parameter for each station analogous to station static corrections for time delays in body wave tomography, except that this site response term is frequency dependent. To account for the scattering effects outside the study regions, a two-plane wave approximation is employed to represent the complexity of the incoming wavefield. The simultaneous inversion for lateral variations in phase velocity, attenuation coefficients, wavefield parameters describing the two-plane waves, and station site responses using many earthquake sources allow us to accurately detect the variation of amplitude due to attenuation within a distance of 1 to 2 wavelengths.

We study a region of very young seafloor in the southeastern Pacific (Fig. 1) in which two ocean-bottom seismometer experiments (OBS) have been conducted. Attenuation is expected to be high due to high temperature in the young oceanic upper mantle and to decrease with distance from the ridge axis due to the cooling of the oceanic lithosphere. For a period of six months in 1995–1996, the Mantle Electromagnetic and Tomography (MELT) seismic team deployed two linear arrays of OBSs (marked with white triangles in Fig. 1) across the southern East Pacific Rise to investigate magma generation beneath mid-oceanic ridges. Rayleigh wave data recorded at as many as 39 stations from 23 earthquakes distributed around the margins of the Pacific have been used to invert for lateral variations in phase velocities [10]. The total number of ray paths employed is 703, but the number of records with good signal-to-noise ratio decreases with increasing period. In a region centered about 400 km west of the East Pacific Rise, the GLIMPSE experiment deployed an array of portable ocean-bottom seismometers for a year located on 4–9 Ma old seafloor including two intraplate volcanic ridge systems, the Sojourn and the Hotu Matua volcanic complexes, to study the origin of gravity lineations and intraplate volcanic ridges on the Pacific plate. 155 events with good signal-to-noise ratios located around the margin of the Pacific plate were recorded at up to 11 stations and used to invert for phase velocities and azimuthal anisotropy [11]. The total number of seismograms we employ from GLIMPSE ranges from a maximum of 1400 at 25 s to 230 at 67 s.

In processing the seismograms, instrument responses are normalized according to provided response parameters. In the MELT experiment, several different types of OBS were deployed. We derived empirical correction

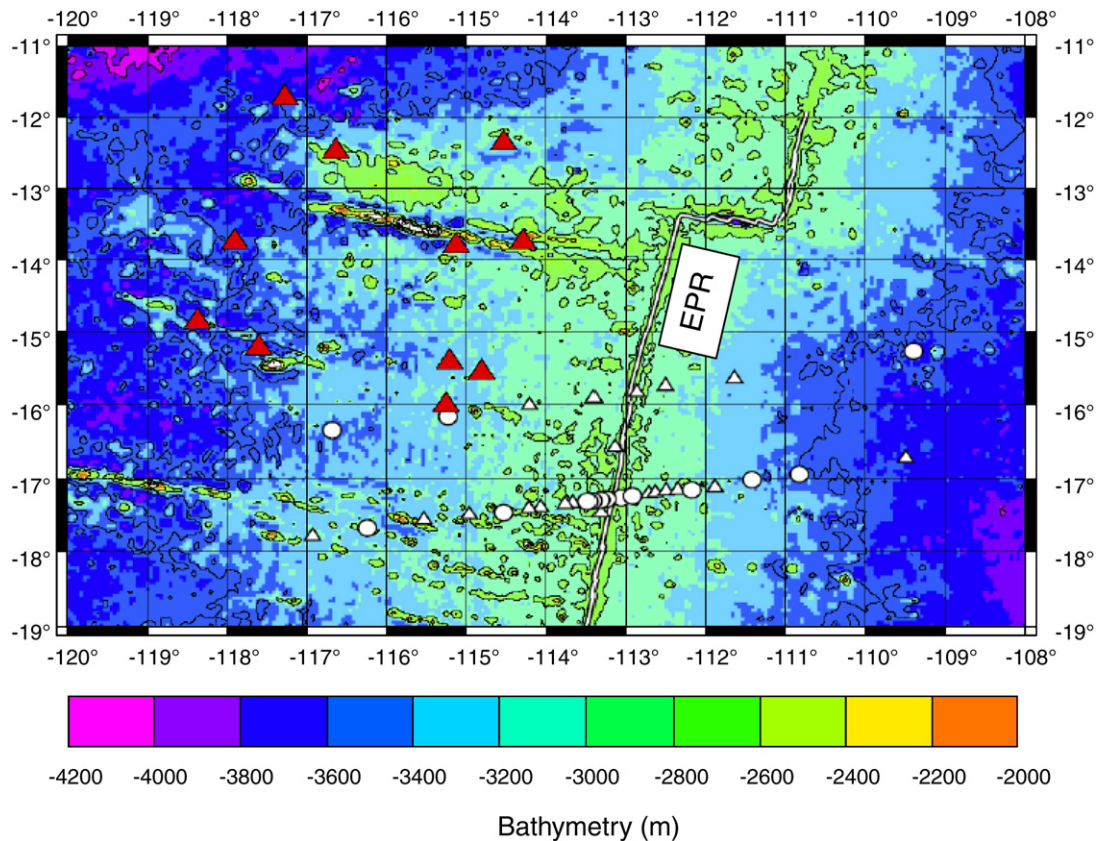


Fig. 1. The bathymetry of the study region. White circles and triangles represent the MELT array and red triangles represent the GLIMPSE array. The East Pacific Rise (EPR) is marked by the double white lines. (For interpretation of the references to colour in this figure legend, the reader is referred to the web version of this article.)

factors for the instrument responses of each group by comparing waveforms at closely spaced stations and by including phase and amplitude correction factors in the inversion. Only vertical components of Rayleigh waves (or in some cases, pressure variations recorded on differential pressure gauges) are used for inversion, since the vertical components have higher signal-to-noise ratio and are not contaminated by Love wave interference. The selected vertical-component seismograms are filtered with a series of narrow-bandpass (10 mHz), zero-phase-shift, Butterworth filters centered at frequencies of interest. All of the filtered vertical-component seismograms are checked individually and only those with signal-to-noise ratio larger than 10 are selected. Fundamental mode Rayleigh waves are isolated from other seismic phases by cutting the seismograms using a boxcar window with a 50-s half cosine taper added to each end. The filtered and windowed seismograms are converted to the frequency domain by Fourier transform to obtain phase and amplitude data. More detailed discussion about the data processing scheme and the meth-

od to perform station corrections is given by Yang and Forsyth [12].

### 3. Results

The effective average age of the seafloor in the MELT study is about 2 Ma versus ~6 Ma in GLIMPSE. Although the two OBS arrays are adjacent, they share no common stations or sources, so we have performed separate inversions. Ray paths for representative periods are shown in Fig. 2. The lateral variations in phase velocity within the study areas are described in other papers [10,11].

To demonstrate that attenuation is resolvable and required by the data, we first perform an inversion with no attenuation factor. The inversion includes the wave parameters that describe interference and amplitude variations due to the complexity of the incoming wave fronts, station site corrections, and phase velocity variations that are adjusted to try to match both the observed phases and the observed amplitudes through



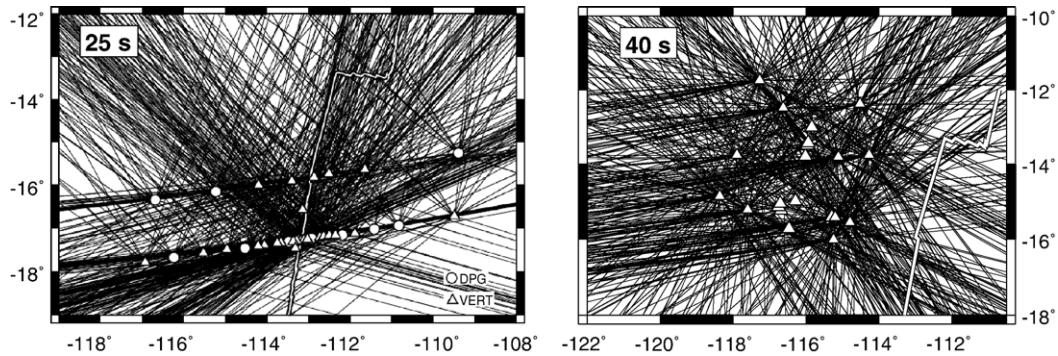


Fig. 2. Great-circle ray paths at a period of 25 s for the MELT array (left) and at a period of 40 s for the GLIMPSE array (right). White triangles and circles represent ocean-bottom seismometers (OBS). The double white lines delineate the East Pacific Rise (EPR).

the effects of focusing. Although a minor effect, the amplitudes are also corrected for the effects of geometrical spreading on a sphere. The observed amplitudes for each event are normalized by the rms value of all observed amplitudes for that event to keep all the amplitudes at the same scale independent of magnitude of the event. We then examine the average residual amplitudes as a function of distance across the array. In Fig. 3, we bin the residuals in 50 km distance intervals measured from the nearest station to each source event for the GLIMPSE array at 16 s period. There is a clear, systematic decrease in residual amplitude with increasing distance from the source, indicating that attenuation is required by the data. The true decay with distance is

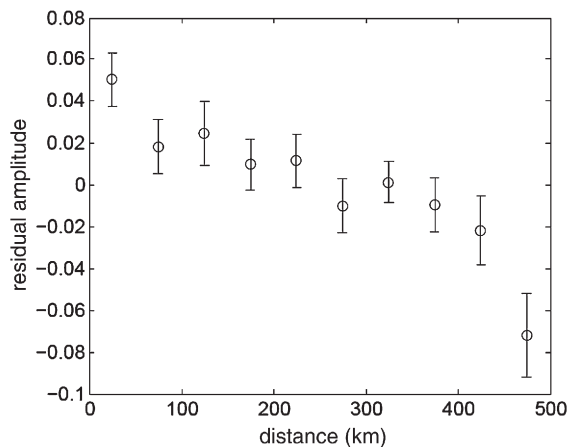


Fig. 3. Variation of residual amplitudes with propagation distance at a period of 16 s in the GLIMPSE region. Each circle represents the average residual amplitude in each 50-km distance interval over all used events. Error bars represent the standard deviations of the average residual amplitudes from an inversion that takes into account focusing, complexity of the incoming wavefield, and station corrections, but ignores attenuation. Note the systematic decay trend of residuals with distance indicating attenuation is required.

somewhat underestimated in this experiment since all the other variables in the inversion have been adjusted as much as possible to match the amplitudes, and, thus, to mimic attenuation with a combination of other effects.

Fig. 4 displays the average attenuation coefficients within the two arrays. Attenuation coefficients at all periods are small, less than  $5 \times 10^{-4} \text{ km}^{-1}$ . At periods shorter than 40 s, attenuation is larger in the MELT region than in the GLIMPSE region. At periods longer than 40 s, attenuation is similar in both regions, although less well-resolved in MELT due to a shorter deployment and higher instrument noise. These observations represent the first measurements of the attenuation of surface waves within regional arrays of seismometers in the oceans.

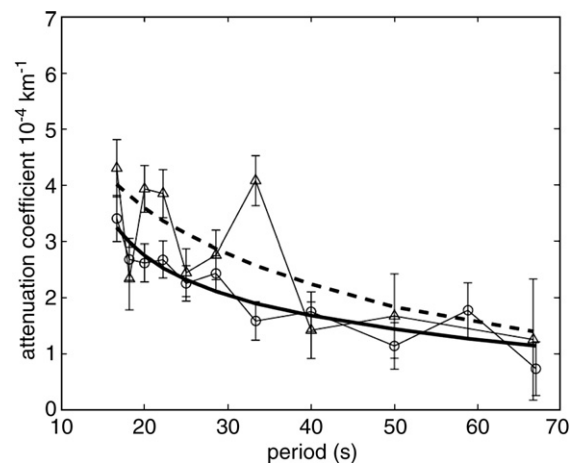


Fig. 4. Attenuation coefficients determined from Rayleigh waves. Thin solid line with circles and thin dashed line with triangles are the observed values for the GLIMPSE array and the MELT array, respectively. Bold solid line and bold dashed line are the predicted values from inverted  $Q_\mu$  model for the GLIMPSE region and the MELT region, respectively.

The attenuation of Rayleigh waves is the integrated effect of intrinsic shear wave quality factor,  $Q_\mu$ , or attenuation  $Q_\mu^{-1}$  over a range of depths, with depth of penetration of the Rayleigh waves increasing with period. The attenuation coefficient of Rayleigh waves at individual periods is represented as a sum of shear wave dissipation ( $Q_{\mu l}^{-1}$ ) in each layer from the surface to great depth as given by,

$$\gamma_R = \frac{\pi}{C_R^2 T} \sum_{l=1}^N \left[ \left( \beta_1 \frac{\partial C_R}{\partial \beta_1} \right)_{\omega \rho \alpha} + \frac{1}{2} \left( \alpha_1 \frac{\partial C_R}{\partial \alpha_1} \right)_{\omega \rho \beta} \right] Q_{\mu l}^{-1} \quad (1)$$

where  $\rho$ ,  $\omega$  and  $l$  are density, angular frequency, and layer number respectively; the partial derivatives of phase velocity,  $C_R$ , with respect to shear velocity,  $\beta$ , or compressional velocity,  $\alpha$ , include both the effects of intrinsic sensitivity and layer thickness [13].

We invert the attenuation coefficients as a function of period for  $Q_\mu$  as a function of depth in the upper mantle. In the inversion, we assume a uniform starting value of 70, compatible with global average values for the low-velocity zone. The particular solution for the GLIMPSE region is shown in Fig. 5. Particular solutions to the inverse problem for  $Q_\mu$  structure may contain features that are suggested, but not required, by oscillations in the data or that are inherited from the starting model. The resolution matrix provides a description of what features of the model are well-resolved. The resolution kernels for selected depths are shown on the right hand

side of Fig. 5. The kernels are reasonably compact, in the sense of not having significant sidelobes, so we can summarize the required features in terms of overlapping averages over resolvable depth ranges, i.e., ranges over which the diagonal elements of the resolution matrix sum to 1.0 pieces of independent information about the system. These resolvable averages and their standard deviations are illustrated in Fig. 6A.

The required features of the attenuation structures are significant decreases in  $Q_\mu$  with increasing depth, greater attenuation beneath the young seafloor of the MELT array than beneath the GLIMPSE, and higher minimum values of  $Q_\mu$  beneath both arrays than are predicted by recent models attributing the origin of the oceanic low-velocity zone to the effects of temperature and anelasticity [6]. Both the increase in attenuation with depth and the decrease associated with the greater average age of the GLIMPSE region suggest that the cooling of the oceanic mantle plays a role, although significant conductive cooling is not expected to extend to depths greater than about 40 km in seafloor younger than 10 Ma. The decrease in  $Q_\mu$  with increasing depth could also be attributed to an increase in water content, as discussed below.

At the 95% confidence level, the average  $Q_\mu$  in the 20–60 km depth range must be greater than about 90 beneath MELT and about 110 beneath GLIMPSE. The best estimates for  $Q_\mu$  in the ~55–120 km depth range are about 79 for MELT and 98 for GLIMPSE, somewhat higher than averages of 60–90 in the asthenosphere in various global 1-D models [14] or the value of 70

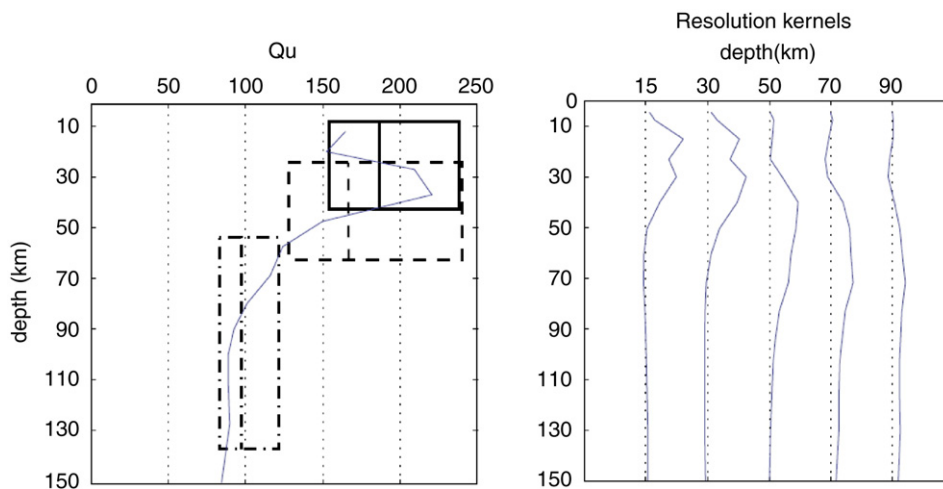


Fig. 5.  $Q_\mu$  model (left) and resolution kernels (right) for the GLIMPSE region. The resolution kernels are plotted for target depths of 15, 30, 50, 70, and 90 km. On the left, the middle line in each rectangle represents the average over the indicated, well-resolved, depth interval. The horizontal extent of each rectangle indicates plus or minus one standard error of the mean. The blue line is the particular solution of  $Q_\mu$ , which has predicted attenuation coefficients shown as the bold solid line in Fig. 4. (For interpretation of the references to colour in this figure legend, the reader is referred to the web version of this article.)

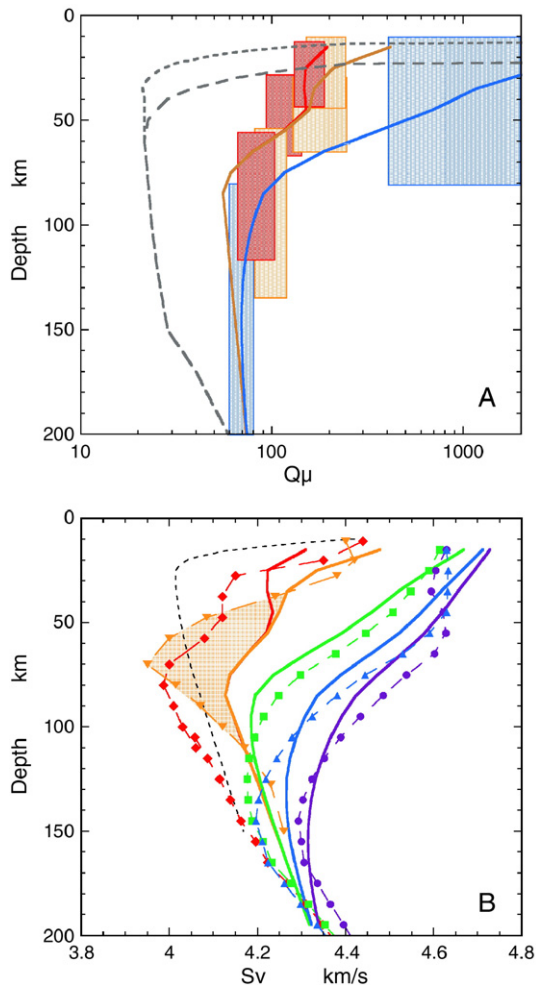


Fig. 6. Quality factor and shear velocity as a function of depth and age of the seafloor. A. Boxes show range of acceptable ( $\pm$  one standard deviation)  $Q_\mu$  averages over resolvable depth ranges. Red, 2 Ma seafloor from MELT array; orange 6 Ma seafloor from GLIMPSE array; blue, average oceanic values assumed to be about 80 Ma. Long dashed line is prediction from [6] for 6 Ma seafloor, short dashed for 2 Ma. Solid red, orange and blue lines are predictions of model described in text for 2 Ma, 6 Ma, and 80 Ma, respectively. B. Shear velocities (SV component) inferred from Rayleigh waves for regions with different average ages. Violet circles, 120 Ma; blue triangles, 80 Ma; green squares, 36 Ma, all from [18]. Orange inverted triangles, 6 Ma; red diamonds, 2 Ma, from this study, except below 100 km from [18]. Corresponding colors in solid curves represent predictions of model described in text for these ages. Orange shaded region illustrates velocity discrepancy between model and observation that we attribute to the presence of melt. Short dashed line is prediction from [6] for 2 Ma. (For interpretation of the references to colour in this figure legend, the reader is referred to the web version of this article.)

obtained for the upper 150 km of the mantle beneath the East Pacific Rise from a study of multibounce SH phases [15]. Although the 95% confidence limits on our values overlap the values in these previous studies, they barely

reach the most likely range estimated by Resovsky et al. [16] for the global average. We speculate that the offset may be caused by the contribution to apparent attenuation from scattering in the global studies, which has relatively little effect on measurements in local, *in situ* arrays like GLIMPSE and MELT if focusing is properly accounted for. A recent global, tomographic model of attenuation considering focusing effects on amplitude [17] finds attenuation at 50 s period on the East Pacific Rise that is  $\sim 17\%$  higher than our estimate for MELT and  $\sim 72\%$  greater than for the off-axis GLIMPSE area. In the period range where the two studies overlap, the values are consistent within their 95% confidence limits, but scattering could still contribute to the greater attenuation in the global study, because it considers only focusing effects from velocity heterogeneities that are at scales resolved in the global tomography. There are strong, short-wavelength heterogeneities resolved within the two regional arrays [10,11] that may contribute to unrecognized scattering.

Shear wave velocities as a function of depth (Fig. 6B) are inverted from the average phase velocities at different periods. A low-velocity zone is observed underlying a high velocity lid with negative gradient. The minimum shear wave velocity reaches 3.9–4.0 km/s at  $\sim 70$ –80 km beneath both arrays. Since the longest period Rayleigh waves are poorly recorded on ocean-bottom seismometers, the resolution of structure is poor below  $\sim 150$  km in GLIMPSE and  $\sim 100$  km in MELT. Shear velocities in the Pacific mantle as a function of seafloor age are also shown from a study of Rayleigh wave propagation covering a broader period range using island and continental stations [18]. The increase in velocity with increasing age of the seafloor has been observed in many studies and is an indication of the gradual cooling and thickening of the oceanic lithosphere.

## 4. Discussions

### 4.1. Problems with thermal models for the origin of the LVZ

Models that attribute the origin of the LVZ to temperature and pressure effects alone can approximately fit the increase in velocities with increasing age by assuming a simple thermal model for the lithosphere and asthenosphere of a cooling half-space [6,7]. These models also predict low attenuation in the cold lithosphere and high attenuation (low  $Q$ ) in the asthenosphere, matching reasonably well the values observed beneath old seafloor in global studies of attenuation [6]. Well-constrained laboratory measurements of the temperature and pressure

dependence of the elastic coefficients of mantle minerals indicate that the anharmonic effects of changing temperature are not sufficient. In order to match the seismic velocities in the LVZ and the low velocities beneath young seafloor, the anelastic, dispersive effects of attenuation are required [5,6]. Attenuation is thermally activated and frequency dependent, usually represented in the form

$$Q^{-1}(\omega, T, P) = A[\omega \exp\{(E + PV)/RT\}]^{-\alpha} \quad (2),$$

where  $\omega$  is angular frequency,  $P$  is pressure,  $T$  is temperature,  $E$  is activation energy,  $V$  is activation volume and  $\alpha$  is a constant that laboratory measurements and seismic observations indicate is between 0.1 and 0.3 [4]. Frequency dependence of attenuation in this power law form leads to frequency dependence of shear velocity  $V_s$  of the form [19],

$$V_s(\omega, T, P) = V_0(T, P) \left[ 1 - \frac{1}{2} \cot\left(\frac{\pi\alpha}{2}\right) Q^{-1}(\omega, T, P) \right] \quad (3),$$

where  $V_0(T, P)$  is the seismic wave velocity including only anharmonic effects.

The problem for these models is that it is necessary to have very high attenuation near mid-ocean ridges to match the large contrast in velocity between old and young seafloors. In Fig. 6A we show that the model of Faul and Jackson [6] predicts  $Q$  values a factor of  $\sim 5$  lower than we observe near the East Pacific Rise, well below the 99% confidence limits in either the 20 to 60 or 55 to 120 km depth ranges under both arrays. Similarly low  $Q$  values are implied by the model of Priestley and McKenzie [7]. We conclude that the temperature dependence of attenuation, and therefore velocity, must be less than predicted in these models. Some other mechanism or mechanisms must be at least partially responsible for the drop in velocity and increase in attenuation beneath the lithosphere in old seafloor and for the variation in velocity with age of the seafloor.

Other than temperature, the two most likely agents for reducing velocity and increasing attenuation are dissolved water in the asthenosphere and interstitial melt beneath the spreading center. The initial formation of the lithosphere probably involves the extraction of water from olivine by partial melting. Since the solubility of water in basaltic melt is 2–3 orders of magnitude greater than in the mantle minerals [20], partial melting above the depth of “dry” solidus ( $\sim 65$  km) and removal of the melt to form the crust at the spreading center can effectively dry out the uppermost mantle. The viscosity of “dry” residuum could be 2 or 3 orders of magnitude

larger than the “damp” peridotite aggregate in the mid-ocean ridge basalt (MORB) source region [20], which could produce a high viscosity lid above the dry solidus at about  $\sim 65$  km beneath young seafloor regions. The observation of an electrically resistive layer overlying an anisotropic, conductive mantle at depths greater than 60 km near the East Pacific Rise strongly supports the interpretation that dissolved water is present in olivine in the asthenosphere, but is absent in the lithosphere [21]. A small degree of melting in the presence of water is expected down to depths of 100 to 150 km beneath the spreading center, but the degree of melting and removal of melt may be too small to effectively dry out the crystals until upwelling reaches the vicinity of the dry solidus.

#### 4.2. A model for the origin of the LVZ

We construct a velocity and attenuation model based on a simple half-space cooling model in which there is a linear transition from dehydrated to damp mantle over the depth range 50 to 80 km. We assume that a small amount of dissolved water affects velocities only through the anelastic attenuation effect, not through a change in elastic coefficients. For simplicity, the enhancement of attenuation from the addition of water is assumed to occur through a change in  $A$  in Eq. (2), amounting to an enhancement of a factor of three from dry to damp, with no change in  $E$ ,  $V$ , or  $\alpha$ . The sensitivity of velocity to a change in temperature is given by

$$\frac{\partial V_s}{\partial T} = \frac{\partial V_0}{\partial T} - V_0 \left[ \frac{\alpha\pi}{2} \cot \frac{\alpha\pi}{2} \frac{Q^{-1}}{\pi} \frac{E + PV}{RT^2} \right]. \quad (4)$$

In our model, the potential temperature at the surface is 1350 °C. The temperature sensitivity is reduced by choosing  $E = 250$  kJ mol $^{-1}$  smaller than in the model of Faul and Jackson [6] and by the decrease  $Q^{-1}$  in associated with dehydration above 80 km. Activation volume is same as in the model of Faul and Jackson with  $V = 1.0 \times 10^{-5}$  m $^3$  mol $^{-1}$ .  $\alpha$  is assigned a minimum value of 0.1 to maximize the effect of a given attenuation on velocity (Eq. (3)). The grain size of upper mantle materials may have some effects on the parameters, in Eq. (2) such as  $A$ ,  $E$ ,  $V$ . But as discussed by Faul and Jackson [6], the variation of grain size above 200 km should be small. Thus we assume the grain size dependent parameters to be the same in our model.

The results are shown in Fig. 6 in comparison to observations of this and other studies. The model agrees reasonably well with the constraints on  $Q$  in both young and older seafloors and with the changes in velocity as a



function of age except beneath young seafloor. Beneath older seafloor, the absolute velocities predicted are a little low in the 40 to 100 km depth range and a little high at greater depths, but the observational constraints are also the result of model inversions of surface wave dispersion data and are somewhat dependent on the starting model and on anisotropy, which we neglect. The major discrepancy between model predictions and the observations is in young seafloor, where the observed velocities at depths of 70 to 80 km are on the order of 0.2 km/s lower than predicted. This is actually a minimum discrepancy, since  $\alpha$  was chosen to maximize the effect of decreasing  $Q$  with age and the velocities in older seafloor at this depth are slightly underpredicted. Any simple thermal model that satisfies the constraints on  $Q$  will not satisfy the minimum velocities observed beneath young seafloor.

We note that the change in velocity with age of the seafloor may actually be somewhat underestimated if SH/SV decreases beneath young seafloor due to more vertical (or less horizontal) alignment of olivine  $a$ -axes associated with upwelling beneath the spreading center [18,22]. More vertical alignment of olivine would increase the Rayleigh wave velocity, thus masking to some extent the velocity decrease beneath the East Pacific Rise compared to older seafloor. The result of neglecting changes in anisotropy would lead to an underestimate of the discrepancy between the observed velocity changes and those predicted by a thermal attenuation model.

We interpret this discrepancy between the observations and predictions as indicating that melt is present beneath young seafloor at concentrations sufficient to affect the seismic velocities. Partial melt has two different effects on seismic velocity: the direct effect due to the difference of elastic properties between melt and solid, and the indirect effects due to enhanced anelasticity, which are already largely accounted for by constructing models that satisfy observed  $Q$ . The anelastic effect depends sensitively on the mechanism of attenuation associated with melting [23–25]. If it is grain boundary sliding, then there is a background effect that is very similar to the effects of increased temperature, plus a broad, frequency-and-temperature dependent absorption peak in the seismic frequency band [23,24]. If it is melt squirt, then the dissipation peak may lie outside the seismic frequency band and cause little attenuation. The direct velocity reduction for melt squirt depends on the aspect ratio of the melt pockets [25]. Direct  $V_s$  reduction per percent partial melt has been estimated to be at least 7.9% for realistic melt distributions [26]. Using this value, the velocity discrepancy

we observe requires on the order of 0.5% melt concentration in the 60 to 80 km depth range and suggests the presence of melt at depths from  $\sim 25$  km to  $\sim 100$  km or more in seafloor averaging 2 Ma in the MELT study area and from  $\sim 40$  km to at least 100 km depth in seafloor of 6 Ma in the GLIMPSE area, about 400 km away from the East Pacific Rift. We note that recent, intraplate volcanism has been found within the GLIMPSE area [27]. The pattern of attenuation and velocity variations with age and depth thus suggests that water is responsible for part of the velocity reduction in the low-velocity zone beneath old seafloor and that partial melt concentrations of at least a few tenths of a percent are responsible for the very low shear velocities beneath mid-ocean ridges.

### Acknowledgements

We would like to thank Uli Faul for the helpful discussions and sharing his codes of the thermal model with us. This research was supported by the National Science Foundation grants OCE-9911729 and EAR-0510621.

### References

- [1] T.J. Shankland, H.S. Waff, Partial melting and elasticity–conductivity anomalies in upper mantle, *J. Geophys. Res.* 82 (1977) 5409–5417.
- [2] M.A. Richards, W.S. Yang, J.R. Baumgardner, H.P. Bunge, Role of a low-viscosity zone in stabilizing plate tectonics: implications for comparative terrestrial planetology, *Geochim. Geophys. Geosyst.* 2 (2001).
- [3] D.L. Anderson, C. Sammis, The low velocity zone, *Geophys. Int.* 9 (1969) 3–19.
- [4] S. Karato, H. Jung, Water, partial melting and the origin of the seismic low velocity and high attenuation zone in the upper mantle, *Earth Planet. Sci. Lett.* 157 (1998) 193–207.
- [5] L. Stixrude, C. Lithgow-Bertelloni, Mineralogy and elasticity of the oceanic upper mantle: origin of the low-velocity zone, *J. Geophys. Res.* 110 (2005) B03204, doi:10.1029/2004JB002965.
- [6] U.H. Faul, I. Jackson, The seismological signature of temperature and grain size variations in the upper mantle, *Earth Planet. Sci. Lett.* 234 (2005) 119–134.
- [7] K. Priestley, D. McKenzie, The thermal structure of the lithosphere from shear wave velocities, *Earth Planet. Sci. Lett.* 244 (2006) 285–301.
- [8] Y. Zhou, F.A. Dahlen, G. Nolet, 3-D sensitivity kernels for surface-wave observables, *Geophys. J. Int.* 158 (2004) 142–168.
- [9] Y. Yang, D.W. Forsyth, Regional tomographic inversion of amplitude and phase of Rayleigh waves with 2-D sensitivity kernels, *Geophys. J. Int.* 166 (2006) 1148–1160.
- [10] D.W. Forsyth, S.C. Webb, L.M. Dorman, Y. Shen, Phase velocities of Rayleigh waves in the MELT experiment on the East Pacific Rise, *Science* 280 (1998) 1235–1238.
- [11] D.S. Weeraratne, D.W. Forsyth, Y. Yang, S.C. Webb, Rayleigh wave tomography of the upper mantle beneath intraplate



- seamount chains in the south Pacific, *J. Geophys. Res.* (in press), doi:10.1029/2006JB004403.
- [12] Y. Yang, D.W. Forsyth, Rayleigh wave phase velocities, small-scale convection and azimuthal anisotropy beneath southern California, *J. Geophys. Res.* 111 (2006) B07306, doi:10.1029/2005JB004180.
- [13] B.J. Mitchell, Anelastic structure and evolution of the continental crust and upper mantle from seismic surface wave attenuation, *Rev. Geophys.* 33 (1995) 441–462.
- [14] B. Romanowicz, J.J. Durek, Seismological constraints on attenuation in the Earth: a review, in: S. Karato, et al., (Eds.), *Earth's Deep Interior, Mineral Physics and Tomography from the Atomic to the Global Scale*, Geophys. Monogr. Ser., vol. 117, AGU, Washington, D.C., 2000, pp. 161–180.
- [15] X.Y. Ding, S.P. Grand, Upper mantle Q structure beneath the East Pacific Rise, *J. Geophys. Res.* 98 (1993) 1973–1985.
- [16] J. Resovsky, J. Trampert, R.D. Van der Hilst, Error bars for the global seismic Q profile, *Earth Planet. Sci. Lett.* 230 (2005) 413–423.
- [17] C.A. Dalton, G. Ekstrom, Global models of surface-wave attenuation, *J. Geophys. Res.* 111 (2006) B05317, doi:10.1029/2005JB003997.
- [18] C.E. Nishimura, D.W. Forsyth, The anisotropic structure of the upper mantle in the Pacific, *Geophys. J.* 96 (1989) 203–229.
- [19] J.B. Minster, D.L. Anderson, A model of dislocation-controlled rheology for the mantle, *Philos. Trans. R. Soc. Lond., A* 299 (1981) 319–356.
- [20] G. Hirth, D.L. Kohlstedt, Water in the oceanic upper mantle: implications for rheology, melt extraction and the evolution of the lithosphere, *Earth Planet. Sci. Lett.* 144 (1996) 93–108.
- [21] R.L. Evans, G. Hirth, K. Baba, D.W. Forsyth, A. Chave, R. Mackie, Geophysical evidence from the MELT area for compositional controls on oceanic plates, *Nature* 437 (2006) 249–252.
- [22] W.C. Hammond, D.R. Toomey, Seismic velocity anisotropy and heterogeneity beneath the Mantle Electromagnetic band Tomography Experiment (MELT) region of the East Pacific Rise from analysis of P and S body waves, *J. Geophys. Res.* 108 (2003) 2176, doi:10.1029/2002JB001789.
- [23] I. Jackson, U.H. Faul, J.D. Fitz Gerald, B.H. Tan, Shear wave attenuation and dispersion in melt-bearing olivine polycrystals: 1. Specimen fabrication and mechanical testing, *J. Geophys. Res.* 109 (2004) B06201, doi:10.1029/2003JB002406.
- [24] U.H. Faul, J.D. Fitz Gerald, I. Jackson, Shear wave attenuation and dispersion in melt-bearing olivine polycrystals: 2. Microstructural interpretation and seismological implications, *J. Geophys. Res.* 109 (2004) B06202, doi:10.1029/2003JB002407.
- [25] H. Schmeling, Numerical experiments on the influence of partial melt on elastic, anelastic, and electric properties of rocks, part I, elasticity and anelasticity, *Phys. Earth Planet. Inter.* 41 (1985) 34–57.
- [26] W.C. Hammond, E.D. Humphreys, Upper mantle seismic wave attenuation: effects of realistic partial melt distribution, *J. Geophys. Res.* 105 (2000) 10,987–10,999.
- [27] D.W. Forsyth, N. Harmon, D.S. Scheirer, R.A. Duncan, Distribution of recent volcanism and the morphology of seamounts and ridges in the GLIMPSE study area: implications for the lithospheric cracking hypothesis for the origin of intraplate, non-hot spot volcanic chains, *J. Geophys. Res.* 111 (2006) B11406, doi:10.1029/2005JB004071.